Error Analysis, Design and Modeling of an Improved Heterodyne Nano-Displacement Interferometer

S. Olyaee* and Sh. Mohammad-Nejad**

Abstract: A new heterodyne nano-displacement with error reduction is presented. The main errors affecting the displacement accuracy of the nano-displacement measurement system including intermodulation distortion error, cross-talk error, cross-polarization error and phase detection error are calculated. In the designed system, a He-Ne laser having three-longitudinal-mode is considered as the stabilized source. The free spectral range of the 35cm laser cavity is about 435-MHz at 632.8-nm wavelength, which a secondary beat frequency equal to 300-kHz is produced by combining the reference and measurement beams. The resolution of the displacement measurement resulting from intermodulation distortion, cross-talk and cross-polarization errors is limited to 18-pm. Also, the phase detection uncertainty causes an error of only 5.9-pm in the displacement measurement. Furthermore, frequency-path models of two- and three-longitudinal-mode laser interferometers are modeled as the ac interference, ac reference, dc interference and optical power terms. A comparison study between two- and three-longitudinal-mode laser interferometers confirms that the performance of the designed system is considerably improved.

Keywords: Cross-Polarization, Frequency-Path Model, He-Ne Laser, Heterodyne Interferometry, Intermodulation Distortion, Nano-Displacement.

1 Introduction

Distance or displacement measurement systems based on the coherent methods provide a high accuracy measurement in different axes [1-7]. The high precision displacement measurement is needed in many applications e.g. Space Interferometry Mission (SIM), scheduled for lunched in 2009, should be repeatedly measure the relative angular position of about 2000 stars to 5prad accuracy over five years [8-9]. This system requires to measure displacement with linearity about 10pm-rms over a distance of several meters. To reach the SIM, various errors in the displacement measurement system should be minimized. On the other hand, the fabrication of semiconductor chips necessarily implies lithographic stepper machines in order to measure high accuracy displacement [10, 11]. Accuracy improvement of the displacement in high velocities causes the minimum feature of the integrated circuits to decrease, and therefore, the number of devices in the substrate will be increased. The laser heterodyne interferometer system is the best choice for these applications.

The basic principals of optical displacement measurement based on interferometer have been presented by Michelson in 1881. The dynamic range and accuracy of displacement measurement were improved by designing the heterodyne interferometers. The basis of classical multiple-wavelength interferometric (MWI) method was described in the 1970s [2]. Frequency and power stabilization, nonlinearities, modeling, implementation and simulation of displacement measurement system using two-mode He-Ne laser were widely presented and discussed [12-16]. The first nanometric displacement measurement system on the basis of three-longitudinal-mode He-Ne laser was reported by Yokoyama et al. in 2001 [17] and then was improved in 2005 [18].

In this paper, we design and analyze a frequency-path model for two- and three-longitudinal-mode heterodyne interferometers. Design and simulation of an electronic section of an improved three-longitudinal-mode laser interferometer are discussed and the main errors including intermodulation distortion, cross-talk, cross-polarization and phase detection errors are also calculated. A comparison study between two- and three-

Iranian Journal of Electrical & Electronic Engineering, 2007.

* The Author is with the Department of Electrical Engineering, Shahid Rajaee Teacher Training University, Lavizan, 16788, Tehran, Iran.
E-mail: s_olyaee@srttu.edu
** The Author is with the Optoelectronic and Laser Laboratory, Department of Electrical Engineering, Iran University of Science and Technology, Tehran, Iran.
E-mail: shahramm@iust.ac.ir

longitudinal-mode laser interferometers is also presented.

2 Principles

The source of the multiple-wavelength interferometer should produce an appropriate emission spectrum including of several discrete and stabilized wavelengths. Some efforts are still being devoted to stabilize three-longitudinal-mode He-Ne lasers [19-21].

The optical frequency differences determine the range of non-ambiguity of distance and the maximum measurable velocity. The stability of the laser source will limit the absolute accuracy of the measurement. On the other hand, the maximal absolute distance which can be measured by multiple-wavelength is limited by the coherence length of the source.

If we consider a two-wavelength interferometry using the optical wavelength λ_1 and λ_2, the phase shift of each wavelength will be

$$\varphi_i = 4\pi d/\lambda_i \qquad (1)$$

where d is the optical path difference and φ_i is the phase shift corresponding to the wavelength λ_i. Therefore, the phase difference between φ_1 and φ_2 is given by:

$$\Delta\varphi = 4\pi d\left(1/\lambda_1 - 1/\lambda_2\right) \qquad (2)$$

And the synthetic wavelength, Λ_{II}, can be expressed as:

$$\Lambda_{II} = \lambda_s = \lambda_1\lambda_2/\left|\lambda_1 - \lambda_2\right| = c/\left|\nu_1 - \nu_2\right| \qquad (3)$$

where ν_1 and ν_2 are the optical frequencies corresponding to λ_1 and λ_2, and c is the velocity of light in vacuum.

The He-Ne laser can be applied to MWI using different laser lines, e.g. at 629.34-nm and 632.8-nm in the two-longitudinal-mode interferometer. This allows us to obtain a synthetic wavelength about 117-μm [22]. Therefore, combining λ_1 and λ_2 and reaching to synthetic wavelength, Λ_{II}, the maximal measurable absolute distance will be increased.

If the number of stabilized wavelengths in the gain curve is increased to three-longitudinal-mode, the synthetic wavelength is obtained as:

$$\Lambda_{III} = \lambda_1\lambda_2\lambda_3/\left|\lambda_1\lambda_2 - 2\lambda_1\lambda_3 + \lambda_2\lambda_3\right| = c/f_b \qquad (4)$$

Therefore, the synthetic wavelength in the three-longitudinal-mode interferometer comparing to two-longitudinal-mode system is considerably increased.

The full width at half maximum (FWHM) gain profile of a He-Ne laser is about 1.5-GHz and the free spectral range (FSR) or mode spacing is obtained as:

$$FSR = c/2L \qquad (5)$$

where L is the cavity length. As a result, the number of standing modes in the gain profile can be adjusted by calibration of the cavity length. Because of a small asymmetry in the gain profile, the unequal primary (inter-mode) beat frequencies ($f_L \neq f_H$) and hence the secondary beat frequency, $f_b = \left|f_L - f_H\right|$, produces.

The error sources in the laser heterodyne interferometer systems includes the non-linearity in the optical section [23, 24], laser intensity fluctuations, laser frequency instability, environmental turbulences, misalignment in the optical instruments, phase detection error, cross-polarization and cross-talk error. Most of them are considered as linear errors that can be reduced or eliminated [25-30].

3 Nano-Displacement Measurement Based on Two- and Three-Longitudinal-Mode Laser Interferometers

The gain profile of the laser output and optical head of the nano-displacement measurement system on the basis of two- and three-longitudinal-mode lasers are shown in Fig. 1. In the both cases, the optical head consists of the *base* and *measurement arms*. First, the laser output is separated by a beam splitter (BS) so the base and measurement beams are produced. Then, the beam is split into two subsequent beams by polarizing beam splitter (PBS) and directed to each path of the interferometers.

Two reflected beams are interfered to each other on the linear polarizer. Because of orthogonally polarized modes, the linear polarizer should be used to interfere two beams as shown in Fig. 2. The stabilized multi-mode He-Ne lasers (having f_1, f_2 and f_3 frequencies in three-mode and having f_1 and f_2 in two-mode) are chosen in which the side modes can be separated from the center mode due to the orthogonal polarization of modes. But in reality, non-orthogonal and elliptical polarization of beams cause each path to contain a fraction of the laser beam belonging to the other path. Hence, the cross-polarization error is produced. In the *reference path* (path.1) of three-longitudinal-mode interferometer, f_1 and f_3 are the main frequencies and f_2 is the leakage one, whereas in the *target path* (path.2), f_2 is the main signal and the others are as the leakages.

The frequency-path models of two- and three-longitudinal-mode interferometers are shown in Fig. 3. In the measurement arm of three-longitudinal-mode interferometer, there are three frequency components and two paths namely the reference and the target (the bold lines are the main signal paths and the dashed lines

are the leakage paths), whereas in two-longitudinal-mode interferometer, there are two frequency components and two paths. The number of active frequency-path elements, n, is obtained by multiplying the number of frequency components by paths. Fig. 4 shows the identification of the physical origin of each frequency-path element for the measurement arms.

The wave intensity being received by an avalanche photodiode (APD) is proportional to the square of the total electrical field and the number of distinct interference terms is equal to $n(n+1)/2 = 21$. In three-longitudinal-mode laser interferometer, the reference path field is obtained as:

$$E_i = E_{i1}\cos(\omega_i t - k_i x_1 + \varphi_{i1}),\ i = 1,2,3 \qquad (6)$$

where φ_{i1} is the initial phases corresponding to the electrical field E_{ij}, k_i is the propagation constant or wave number $(2\pi/\lambda_i)$, and x_1 is the motion of the corner cube prism in the reference path (CCP.1). Similar to Eq. (6), the target path field is described by:

$$E_i = \tilde{E}_{i2}\cos(\omega_i t - k_i x_2 + \varphi_{i2}),\ i = 1,2,3 \qquad (7)$$

where x_2 is the motion of the corner cube prism in the target path (CCP.2). In this system, the CCP.1 is fixed and hence, $x_1 = 0$. Furthermore, the wavelengths are so close that propagation constants become almost equal to each other $(k_1 = k_2 = k_3 = k)$.

By squaring the total fields, the photocurrent of the avalanche photodiode is given as:

$$I_{APD} \propto \left(\sum_{i=1}^{6} E_i\right)^2 \qquad (8)$$

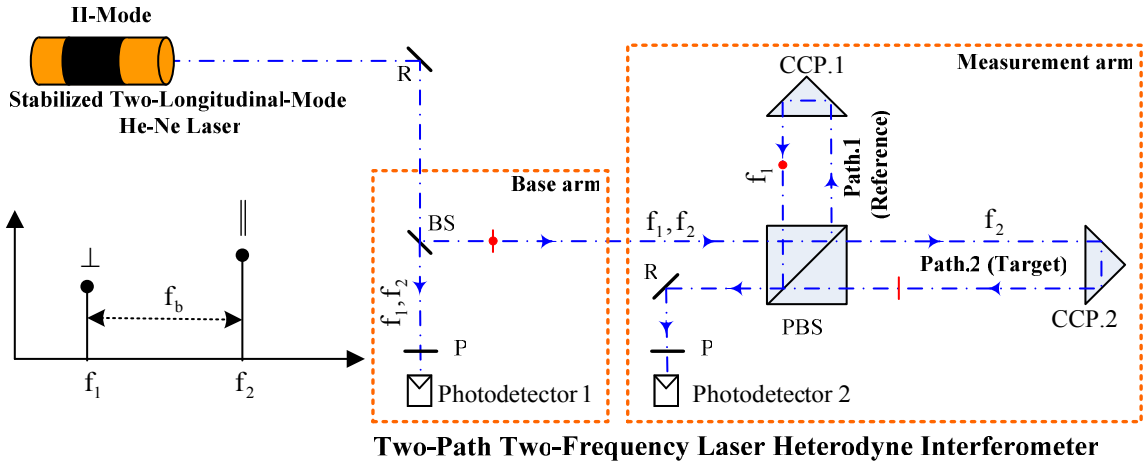

(a)

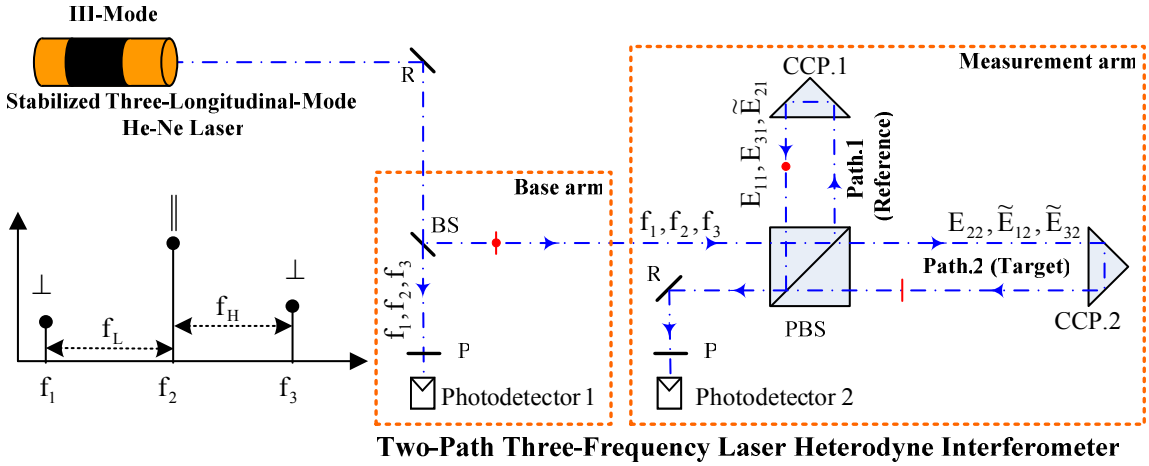

(b)

Fig. 1 The gain profile and optical head of the nano-displacement measurement system based on the two-longitudinal-mode (top) and three-longitudinal-mode (bottom) He-Ne laser interferometers. PBS: polarizing beam splitter; CCP: corner cube prism; BS: beam splitter.

The high frequency components such as ω_i, $2\omega_i$, and $\omega_i+\omega_j$ are eliminated by the avalanche photodiode $(i,j=1,2,3)$. Therefore, ignoring the high frequencies in the fully unwanted leaking interferometers, there are 21 distinct interference terms for three-longitudinal-mode interferometer and 10 distinct interference terms for two-mode type.

The distinct interference terms can be divided into four groups namely *dc interference*, *ac interference*, *ac reference*, and *optical power* [31]. These components in the three-longitudinal-mode interferometer are respectively given by:

$$I_{DI}/K = E_{11}\tilde{E}_{12}\cos(kx_2)+\tilde{E}_{21}E_{22}\cos(kx_2)+E_{31}\tilde{E}_{32}\cos(kx_2) \quad (9)$$

$$\begin{aligned} I_{AI}/K = {} & E_{11}E_{22}\cos(\omega_L t-kx_2)+E_{11}\tilde{E}_{32}\cos((\omega_H+\omega_L)t-kx_2)+\\ & \tilde{E}_{21}\tilde{E}_{12}\cos(\omega_L t+kx_2)+\tilde{E}_{21}\tilde{E}_{32}\cos(\omega_H t-kx_2)+\\ & E_{31}\tilde{E}_{12}\cos((\omega_H+\omega_L)t+kx_2)+E_{31}E_{22}\cos(\omega_H t+kx_2) \end{aligned} \quad (10)$$

$$\begin{aligned} I_{AR}/K = {} & E_{11}\tilde{E}_{21}\cos(\omega_L t)+\tilde{E}_{21}E_{31}\cos(\omega_H t)+\\ & \tilde{E}_{12}E_{22}\cos(\omega_L t)+E_{22}\tilde{E}_{32}\cos(\omega_H t)+\\ & \tilde{E}_{12}\tilde{E}_{32}\cos((\omega_L+\omega_H)t)+E_{11}E_{31}\cos((\omega_L+\omega_H)t) \end{aligned} \quad (11)$$

$$I_{OP}/K = \frac{1}{2}\sum_{j=1}^{2}\sum_{i=1}^{3}E_{ij}^2 \quad (12)$$

Figure 5 shows the combination of the frequency-path elements in the measurement arm of two systems. The main signals and leakages are depicted by large and small solid circles, respectively. On the other hand, the diameter of the circles presents the amplitude of the signals. The small solid circles are exaggerated for clarification. All of the distinct interference terms are shown in Fig. 5 by different lines.

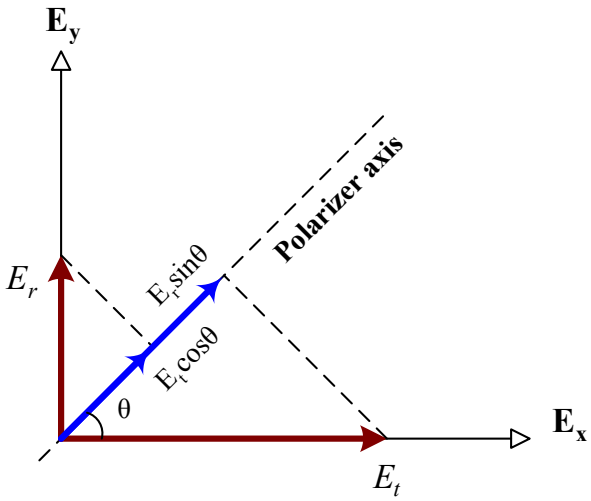

Fig. 2 Combination of orthogonally polarized beams on the linear polarizer.

4 System Design

As shown in Fig. 1, the incident optical power is converted to photocurrent signal by two avalanche photodiodes. The schematic of the electronic section of the designed system is shown in Fig. 6 for three-longitudinal-mode laser interferometer. According to the figure, the photocurrent of the avalanche photodiodes is converted to voltage and amplified by two current to voltage converters (IVC_1 and IVC_2) and low noise amplifiers (A_1 and A_2), respectively.

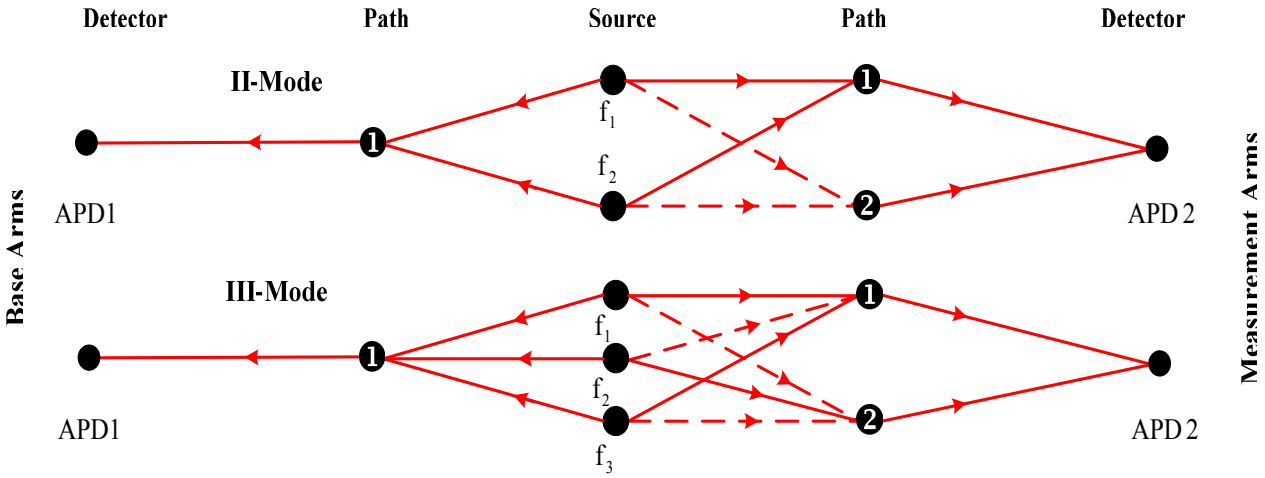

Fig. 3 The frequency-path model in two- and three-longitudinal-mode laser interferometers.

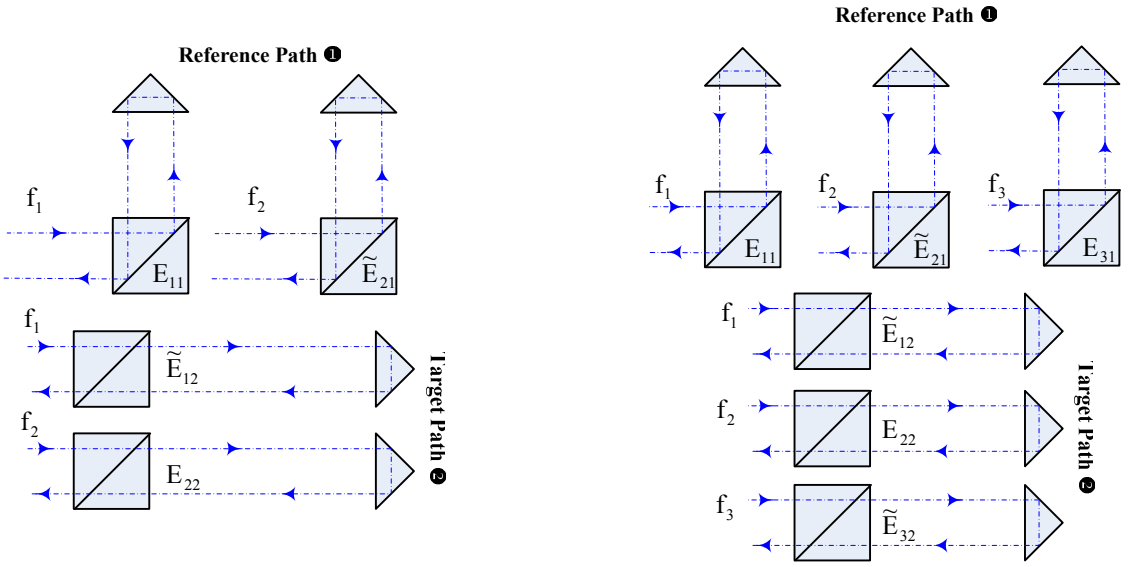

Fig. 4 Identification of the physical origin of each frequency-path element in the reference and target paths (measurement arms). (a) Two- and (b) Three-longitudinal-mode laser interferometers.

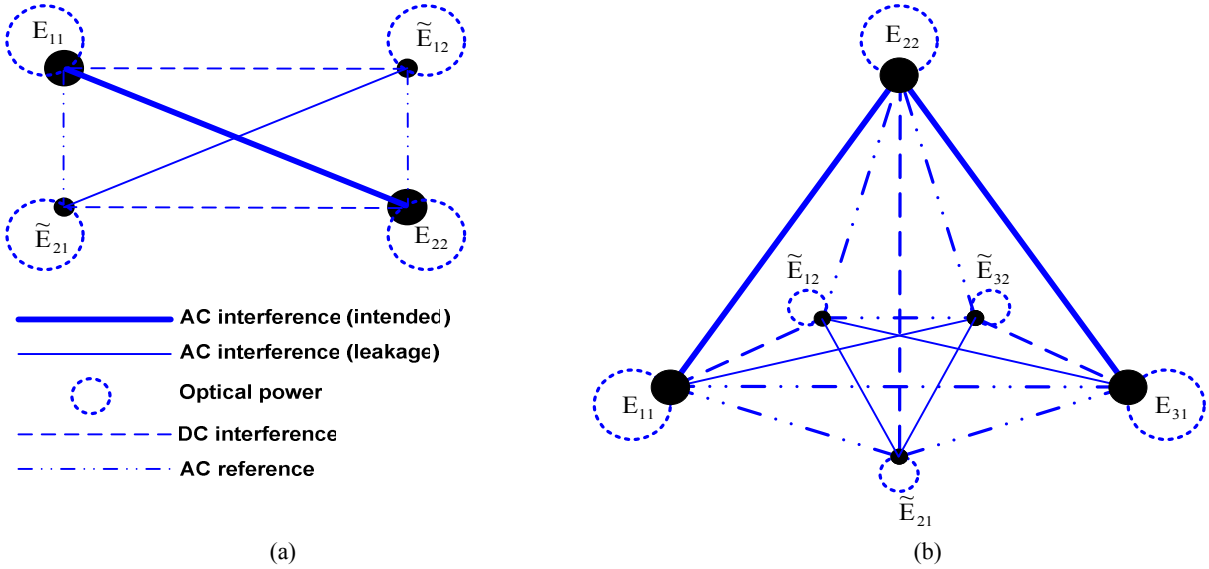

Fig. 5 The combination graph of the frequency-path elements in (a) two-longitudinal-mode and (b) three-longitudinal-mode interferometers.

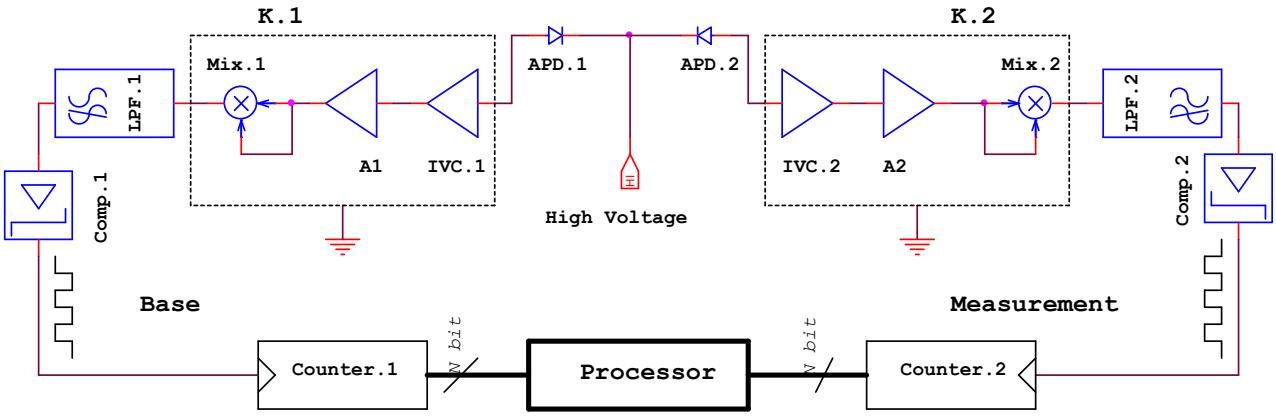

Fig. 6 The schematic of the electronic section of the designed nano-displacement measurement system based on the three-longitudinal-mode laser interferometer.

The unwanted electrical induction between the base and measurement paths can be reduced by using two isolated power supplies for APD biasing and by separating the grounds (analog-base, analog-measurement and digital grounds). Furthermore, because of switching noise of digital section including frequency and phase measurement circuits and microcontroller, two high-speed opto-couplers isolate the analog circuits from digital section. Fig. 7 shows the designed circuit with cross-talk error reduction.
The non-leakage base and measurement signals at the end of the amplifiers are respectively described by:

$$v_{bas} = A\cos\left((\omega_H + \omega_L)t\right) + B\cos(\omega_H t) + C\cos(\omega_L t) + D \quad (13)$$

$$v_{mea} = A'\cos\left((\omega_H \mp \Delta\omega)t - \Phi\right) + B'\cos\left((\omega_L \pm \Delta\omega)t + \Phi\right) + C'\cos\left((\omega_H + \omega_L)t\right) + D' \quad (14)$$

where $\Delta\omega$ is the frequency shift due to the Doppler effect $(\Delta\omega = kx/t)$ which can be calculated as:

$$\Delta\omega = 2\pi\left(2n\overline{V}/\lambda_2\right) \quad (15)$$

where λ_2 is the central wavelength, n is the refractive index of the medium and $\overline{V}$ is the target velocity.
The represented signals in Eqs. (13-14) will be self-multiplied by two double-balanced mixers (Mix_1 and Mix_2). The secondary beat frequency in the base and measurement arms are extracted by two low pass filters (LPF) whose cut off frequency is 550kHz. The secondary beat frequency is clearly much smaller than the others $(f_b << f_H, f_L)$. Therefore, the output signals of the low pass filters for the base and measurement arms are written as:

$$V_{o_{bas}} = G_1\cos(2\pi f_b t + \varphi) \quad (16)$$

$$V_{o_{mea}} = G_2\cos\left(2\pi\left(f_b \pm \frac{4n\overline{V}}{\lambda_2}\right)t - 2\Phi + \varphi\right) \quad (17)$$

where G_1 and G_2 are the total gain of the current to voltage converter, low noise amplifier (see Fig. 8a), double-balanced mixer and low pass filter for the base and measurement arms, respectively. The above sinusoidal signals are converted to square waveform. Then, the secondary beat frequency is measured by a high bandwidth up/down counter. As a result, the Doppler shift frequency is measured. If the counted frequency resulting from the Doppler shift frequency is denoted as N, the displacement is given by [4]:

$$\Delta d = \frac{\lambda}{4}\left[N + \frac{\Phi_2 - \Phi_1}{2\pi}\right] \quad (18)$$

The fractional term of Eq. (18) is obtained by measuring the initial and final phases between the base and measurement signals (Φ_1 and Φ_2) by an accurate phase detector. Fig. 9 shows the Doppler shift frequency and phase shift in terms of nanometric displacement. The operation of phase detector is important, especially in the lower velocities. The phase detection method has been used in conventional interferometers and there are many techniques for phase detection such as averaging of the pulse width, triangular wave generation, Vernier scheme, etc. [32]. The phase measurement circuit is shown in Fig. 8(b). In this circuit, the base and measurement signals are exerted to a half exclusive-or gate and the pulse width is measured by a high speed counter. The resolution of the phase detector is proportional to clock pulse of the counter. Here, we suggest a universal time-to-digital converter TDC-GP1 as a high speed counter which can be also used as a frequency measurement device. The phase difference between the base and measurement signals is proportional to the output pulse width. For frequency measurement, the signal must be exerted simultaneously to the stop and start inputs. The maximum pulse width is $1/2f_b$ and the phase detection resolution is obtained as:

$$\delta_\Phi = 2\pi f_b / f_{TDC} \quad (19)$$

where $f_{TDC} = 8\,GHz$.
In summary, by measuring the shifted frequency $(f_b \pm 2\Delta f)$, the velocity of the target (CCP_2) will be obtained. Also, and the displacement of the target can be calculated by integrating the velocity or by measuring the phase -2Φ, $(\Phi = 4\pi d/\lambda_2)$.

5 Error Analysis

Considering 35-cm cavity length for He-Ne laser at 632.8-nm, the free spectral range is obtained from Eq. (5) as 428.275-MHz. The full width at half maximum of He-Ne laser is about 1.5-GHz and hence three stabilized modes can be found in the gain curve. Assuming the primary beat frequencies to be equal to 435.00-MHz and 435.30-MHz, the secondary beat frequency becomes 0.30-MHz [17, 18]. The maximum measurable velocity is limited by the secondary beat frequency and from Eq. (15) is given as:

$$\begin{aligned} &\omega = 2\pi \times 2n\overline{V}/\lambda_2 \\ &\underbrace{2\Delta\omega_{max} = 2\pi f_b} \\ &\overline{V}_{max} = f_b.\lambda_2/4n\Big|_{n=1} \end{aligned} \quad (20)$$

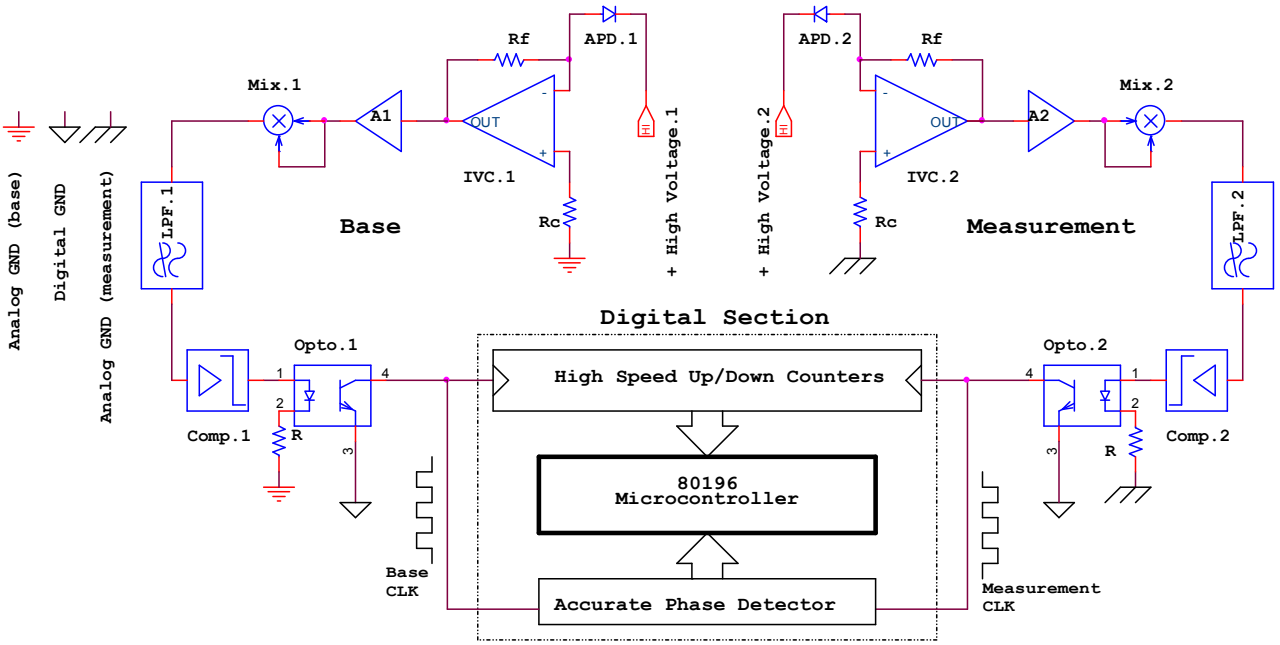

Fig. 7 The schematic of the electronic section of the designed nano-displacement measurement system with cross-talk reduction.

The main sources that affect the accuracy of the three-longitudinal-mode interferometer are as follows:

a. The cross-polarization error

The unwanted optical leakage of the reference and target paths causes cross-polarization error. For a fixed target, the ac interference and the ac reference components are coincident and the mode spacing is equal to the secondary beat frequency, 300-kHz. The ac reference terms, Eq. (11), don't change with variation of the target velocity.

The maximum measurable velocity corresponding to Eq. (20) becomes 47.46-mm/s. In the lower velocity, the frequencies of the ac and dc interference are slightly shifted. However, reduction of the primary to the secondary beat frequency causes the maximum measurable velocity to be considerably reduced.

b. The intermodulation distortion error

The amplification and self-multiplication of the signal produce the nonlinear components. So, in addition to the main signal, there will be higher order harmonics.

c. The phase detection error

The displacement measurement can be limited by the accuracy of the phase measurement. As mentioned previously, by using the high-speed counter as shown in Fig. 8(b), the phase detection resolution is equal to 0.014^{o} and the displacement error due to the deviation of the phase detection is limited to 5.93-pm.

d. The cross-talk error

The combining the reference and target fields, the phase between them is shifted by:

$$\Psi_{err} = \theta_o - \Psi_o = \arctan\left(-I_{ol}/I_{ot}\right) \qquad (21)$$

where θ_o is the measurement phase, Ψ_o is the real phase, I_{ot} and I_{ol} are the main signal and leakage amplitudes, respectively. The amplitude of the measurement signal is given by:

$$I_{om} = \left(I_{ol}^2 + I_{ot}^2 + 2I_{ol}I_{ot}\cos\Psi_{err}\right)^{1/2} \qquad (22)$$

Therefore, the phase error and hence the systematic errors can be increased by increasing the leakage amplitude as shown in Fig. 10. The signal to leakage ratio is also defined by:

$$SLR = \frac{I_{ot}}{\left(\sum_{i=1}^{n} I^2_{ol_i}\right)^{1/2}} \qquad (23)$$

where I_{ot} and I_{ol_i} are the amplitude of the main signal and the i^{th} leakage, respectively.

Since the detected phase is changed by leakage, the error in the nanometric displacement measurement (δ_d) can be written as:

$$\delta_{d_l} = \lambda/4\left[\tan^{-1}\left(I_{ol}/I_{ot}\right)/2\pi\right] \qquad (24)$$

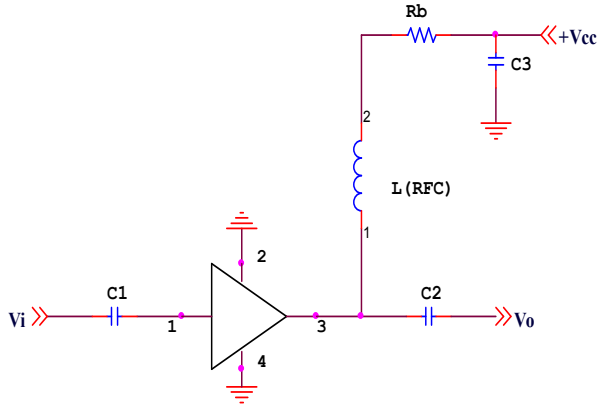

(a)

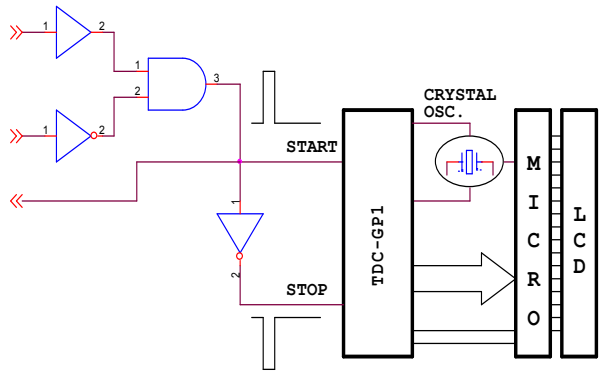

(b)

Fig. 8 (a) The low noise amplifier and (b) the phase measurement circuit.

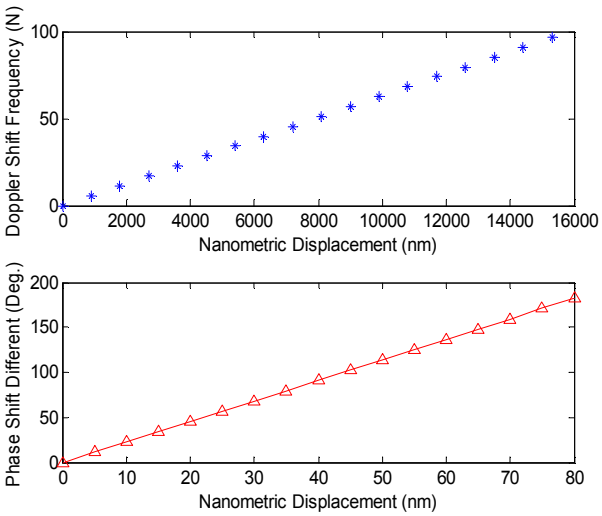

Fig. 9 The Doppler shift frequency and phase shift in terms of nano-displacement.

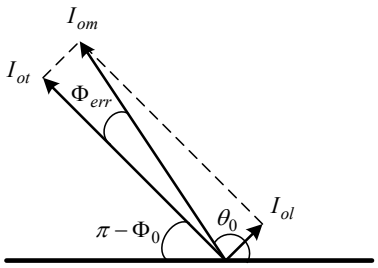

Fig. 10 Phase shift error resulting from leakage.

Table 1 A comparison between two- and three-longitudinal-mode He-Ne laser interferometers.

Parameter		Two-Longitudinal-Mode Laser Interferometer		Three-Longitudinal-Mode Laser Interferometer		Unit
Wavelength		632.8		632.8		nm
Cavity length		25		35		cm
Synthetic wavelength		0.5		1000		m
Maximum absolute distance		0.25		500		m
Intermode beat frequency		600		435.00, 435.30, 870.30		MHz
Secondary beat frequency		---		300		kHz
Maximum measurable velocity		21		0.047		m/s
Phase detection accuracy (similar circuit)		11.8		5.9		pm
Cross-talk and intermodulation distortion error		100		18		pm
The number of active frequency-path elements		4		6		
The number of distinct interference terms	Optical power	Total: 10	4	Total: 21	6	
	AC interference		2		6	
	DC interference		2		3	
	AC reference		2		6	

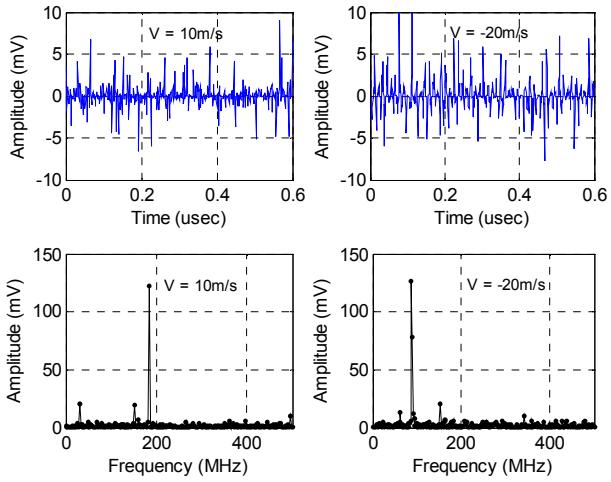

(a)

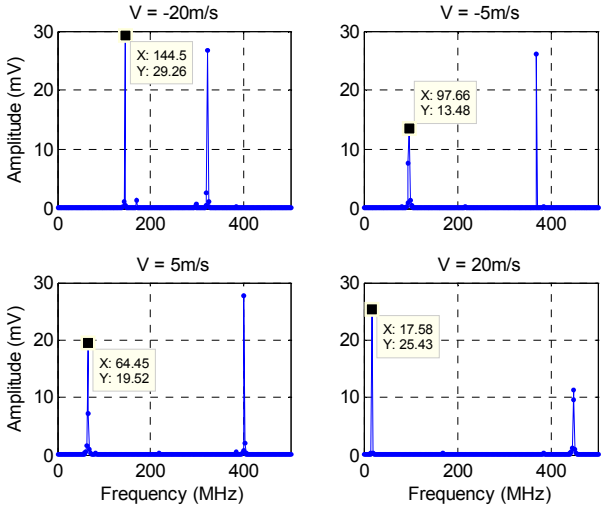

(b)

Fig. 11 The measured signals (a) before and (b) after the noise and cross-talk reduction (heterodyne technique).

The measured signals before and after the noise and cross-talk reduction for two-longitudinal-mode interferometer are shown in Fig. 11. Similarly, the results of the simulations indicate that the signal to leakage and intermodulation distortion ratio before and after the noise and cross-talk reduction for three-longitudinal-mode interferometer are about 17-dB and 63-dB, respectively.

As a result, accuracy of the nanometric displacement due to the cross-talk error and intermodulation distortion reaches about 0.018-nm.

However, the cross-talk and intermodulation distortion errors can be dominated and as a result the displacement resolution can be limited to 18-pm without nonlinearity consideration.

By comparing two-longitudinal-mode interferometer with three-longitudinal-mode interferometer, we will see that the displacement measurement resolution is doubled. Comparison data of these systems are described in Table 1. Although the maximum measurable velocity in three-mode is dramatically reduced, the displacement resolution due to the phase detection error is doubled and the beat frequency is considerably decreased. Also, the maximum absolute distance is improved by a factor of 2000.

6 Conclusion

The frequency-path models of the heterodyne nano-displacement interferometers based on the two- and three-longitudinal-mode He-Ne lasers have been presented. These models described the ac reference, ac interference, dc interference and optical power components of the interferometers. Also, the system performance was improved by reduction of main errors including the phase detection uncertainty, intermodulation distortion, cross-polarization and cross-talk errors. The displacement resolution limited by intermodulation distortion, cross-polarization and cross-talk errors was calculated as 18-pm. In addition, the phase detection uncertainty causes 5.9-pm error in the displacement measurement. Finally, a comparison between two-longitudinal-mode and three-longitudinal-mode heterodyne interferometers confirms that the displacement resolution due to the phase detection error was doubled in three-longitudinal-mode heterodyne interferometer.

Acknowledgement

The authors would like to thank Iran Telecommunication Research Center (ITRC) for financial support.

References

[1] Chassagne L., Topcu S., Alayli Y. and Juncar P., "Highly accurate positioning control method for piezoelectric actuators based on phase-shifting optoelectronics," *Meas. Sci. Technol.*, Vol. 16, pp. 1771–1777, 2006.

[2] Kim M. and Kim S., "Two-way frequency-conversion phase measurement for high-speed and high-resolution heterodyne interferometry," *Meas. Sci. Technol.*, Vol. 15, pp. 2341–2348, 2004.

[3] Yokoyama S., Ohnishi J., Iwasaki S., Seta K., Matsumoto H. and Suzuki N., "Real-time and high-resolution absolute-distance measurement using a two-wavelength superheterodyne interferometer," *Meas. Sci. Technol.,* Vol. 10, pp. 1233–1239, 1999.

[4] Yim N., Eom C. and Kim S., "Dual mode phase measurement for optical heterodyne interferometry," *Meas. Sci. Technol.*, Vol. 11, pp. 1131–1137, 2000.

[5] Ma L. S. and Hall J. L., "Optical heterodyne spectroscopy enhanced by an external optical cavity: toward improved working standards," *IEEE J. Quantum Electron,* QE-26, pp. 2006-2012, 1990.

[6] Yokoyama T., Yokoyama S., Yoshimori K. and Araki T., "Sub-nanometre double shearing heterodyne interferometry for profiling large scale planar surfaces," *Meas. Sci. Technol*., Vol. 15, pp. 2435–2443, 2004.

[7] Demarest F. C., "High-resolution, high-speed, low data age uncertainty, heterodyne displacement measuring interferometer electronics," *Meas. Sci. Technol.*, Vol. 9, pp. 1024–1030, 1998.

[8] Halverson P. G. and Spero R. E., "Signal processing and testing of displacement metrology gauges with picometre-scale cyclic nonlinearity," *J. Opt. A: Pure Appl. Opt*., Vol. 4, pp. S304–S310, 2002.

[9] http://sim.jpl.nasa.gov, accessed January 2008.

[10] Gilsinn J., Zhou H., Damazo B., Fu J. and Silver R., "Nano-lithography in ultra-high vacuum (UHV) for real world applications," *Proc. Nanotech 2004*, Boston, 2004.

[11] Brink M., Jasper H., Slonaker S., Wijnhoven P. and Klaassen F., "Step-and-scan and step-and-repeat; a technology comparison," *Proc. SPIE,* 2726 pp. 734–53, 1996.

[12] Eom T. B., Choi H. S. and Lee S. K., "Frequency stabilization of an internal mirror He–Ne laser by digital control," *Rev. Sci. Instrum*., Vol. 73, pp. 221-224, 2002.

[13] Huang T. L., Chen Y. S., Shy J. T. and Liu H. P., "Two-mode frequency stabilization of an internal-mirror 612 nm He-Ne laser," *Proc. Natl. Sci. Counc. ROC(A)*, Vol. 24, No. 4, pp. 274-278, 2000.

[14] Wu C., "Periodic nonlinearity resulting from ghost reflections in heterodyne interferometry," *Optics Communications*, Vol. 215, pp. 17–23, 2003.

[15] Olyaee S. and Mohammad Nejad S., "Nonlinearity and frequency-path modelling of three-longitudinal-mode nanometric displacement measurement system," *IET Optoelectronics*, Vol. 1, No. 5, pp. 211-220, 2007.

[16] Cosijns S. J., Haitjema H. and Schellekens P. H., "Modeling and verifying non-linearities in heterodyne displacement interferometry," *Precision Eng*., Vol. 26, pp. 448–455, 2002.

[17] Olyaee S. and Mohammad Nejad S., "Design and simulation of velocity and displacement measurement system with subnanometer uncertainty based on a new stabilized laser Doppler-interferometer," *The Arabian Journal for Science and Engineering,* Vol. 32, No. 2C, pp. 89-99, 2007.

[18] Yokoyama S., Yokoyama T. and Araki T., "High-speed subnanometre interferometry using an improved three-mode heterodyne interferometer," *Meas. Sci. Technol*., Vol. 16, pp. 1841–1847, 2005.

[19] Suh H. S., Yoon T. H., Chung M. S. and Choi O. S., "Frequency and power stabilization of a three longitudinal mode He-Ne laser using secondary beat frequency," *Appl. Phys. Lett.* Vol. 63, pp. 2027-2029, 1993.

[20] Yeom J. Y. and Yoon T. H., "Three-longitudinal-mode He–Ne laser frequency stabilized at 633 nm by thermal phase locking of the secondary beat frequency," *Appl. Opt.,* Vol. 44, No. 2-10, 2005.

[21] Olyaee S. and Mohammad Nejad S., "Stabilization of laser frequency based on the combination of frequency locking and power balance methods," *J. Appl. Sci*., Vol. 7, No. 24, pp. 3965-3970, 2007.

[22] Dandliker R., Hug K., Politch J. and Zimmermann E., "High-accuracy distance measurements by multiple-wavelength interferometry," *Opt. Eng*. Vol. 34 (8), pp. 2407-2412, 1995.

[23] Eom T. B., Kim J. Y. and Jeong K., "The dynamic compensation of nonlinearity in a homodyne laser interferometer," *Meas. Sci. Technol*. Vol. 12, pp. 1734–1738, 2001.

[24] Olyaee S. and Mohammad Nejad S., "Characterization of elliptically polarized light and rotation angle of PBS in the three-longitudinal-mode laser interferometer using the Jones matrices," *J. Appl. Sci*., Vol. 7, No. 19, pp. 2806-2811, 2007.

[25] Robertson D., Killow C., Ward H., Hough J., Heinzel G., Garcia A., Wand V., Johann U. and Braxmaier C., "LTP interferometer-noise sources and performance," *Class. Quantum Grav*., Vol. 22, pp. 155–163, 2005.

[26] Wand V., Bogenstah J., Braxmaier C., Danzmann K., Garcıa A., Guzman F., Heinzel G., Hough J., Jennrich O., Killow C., Robertson D., Sodnik Z., Steier F. and Ward H., "Noise sources in the LTP heterodyne interferometer," *Class. Quantum Grav*. Vol. 23, pp. 159–167, 2006.

[27] Chang H. F., Chou C., Teng H. K., Wu H. and Yau H., "The use of polarization modulation and amplitude-sensitive optical heterodyne interferometry for linear birefringence parameters measurement," *Optics Communications*, Vol. 260, pp. 420–426, 2006.

[28] Meyers J. F., Lee J. W. and Schwartz R. J., "Characterization of measurement error sources in Doppler global velocimetry," *Meas. Sci. Technol*., Vol. 12, pp. 357–368, 2001.

[29] Sutton C. M., "Nonlinearity in the length measurement using heterodyne laser Michelson interferometry," *J. Phys. E: Sci. Instrum*., Vol. 20, pp. 1290–2, 1987.

[30] Hou W. and Wilkening G., "Investigation and compensation of the nonlinearity of heterodyne interferometers," *Precision Eng*., Vol. 14, pp. 91–8, 1992.

[31] Schmitz T. and Beckwith J. F., "An investigation of two unexplored periodic error sources in differential-path interferometry," *Precision Eng*., Vol. 27, pp. 311–322, 2003.

[32] Lio H. P. and Young M. S., "New digital phase meter concept and its application," *Rev. Sci. Instrum*., Vol. 68, pp.1894–901, 1997.

Saeed Olyaee was born in Mashhad, Iran, in 1975. He received the B.Sc. degree in Electrical Engineering from University of Mazandaran, Babol, Iran, in 1997 and the M.Sc. and the Ph.D. degrees in Electrical Engineering specializing in Optoelectronics from Iran University of Science and Technology, Tehran, Iran, in 1999 and 2007, respectively. His doctoral dissertation concerned nanometric displacement measurement based on three-longitudinal-mode laser. Currently, he is an Assistant Professor in Department of Electrical Engineering, Shahid Rajaee University, Tehran, Iran. Dr. Olyaee's main research interests include nanodisplacement measurement, optical instrumentation and optoelectronic circuits.

Shahram Mohammad-Nejad received his B.Sc. in Electrical Engineering from University of Houston, Houston, USA, in 1981 and M.Sc. and Ph.D. degrees in Semiconductor Material Growth and Lasers from Shizuoka University, Shizuoka, Japan, in 1990 and 1993, respectively. Professor Mohammad-Nejad invented the PdSrS laser for the first time in 1992. He has published over 80 scientific papers and books. Currently, he is the Head of Electrical Engineering Department, Iran University of Science and Technology, Tehran, Iran. Also, he is a scientific committee member of Iranian Conference of Electrical Engineering (ICEE), member of Institute of Engineering and Technology (IET) and an IET-CEng. His research interests include semiconductor material growth, quantum electronics, semiconductor devices, optoelectronics, electronic devices and lasers.